



## Black silicon laser-doped selective emitter solar cell with 18.1% efficiency

**Davidson, Rasmus Schmidt; Li, Hongzhao; To, Alexander ; Wang, Xi; Han, Alex; An, Jack; Colwell, Jack; Chan, Catherine; Wenham, Alison; Schmidt, Michael Stenbæk**

*Total number of authors:*

14

*Published in:*

Solar Energy Materials & Solar Cells

*Link to article, DOI:*

[10.1016/j.solmat.2015.10.018](https://doi.org/10.1016/j.solmat.2015.10.018)

*Publication date:*

2016

*Document Version*

Peer reviewed version

[Link back to DTU Orbit](#)

*Citation (APA):*

Davidson, R. S., Li, H., To, A., Wang, X., Han, A., An, J., Colwell, J., Chan, C., Wenham, A., Schmidt, M. S., Boisen, A., Hansen, O., Wenham, S., & Barnett, A. (2016). Black silicon laser-doped selective emitter solar cell with 18.1% efficiency. *Solar Energy Materials & Solar Cells*, 144, 740-747.  
<https://doi.org/10.1016/j.solmat.2015.10.018>

---

### General rights

Copyright and moral rights for the publications made accessible in the public portal are retained by the authors and/or other copyright owners and it is a condition of accessing publications that users recognise and abide by the legal requirements associated with these rights.

- Users may download and print one copy of any publication from the public portal for the purpose of private study or research.
- You may not further distribute the material or use it for any profit-making activity or commercial gain
- You may freely distribute the URL identifying the publication in the public portal

If you believe that this document breaches copyright please contact us providing details, and we will remove access to the work immediately and investigate your claim.

# Black Silicon Laser-Doped Selective Emitter Solar Cell with 18.1% Efficiency

Rasmus Schmidt Davidsen<sup>a,\*</sup>, Hongzhao Li<sup>c</sup>, Alexander To<sup>c</sup>, Xi Wang<sup>c</sup>, Alex Han<sup>c</sup>, Jack An<sup>c</sup>, Jack Colwell<sup>c</sup>, Catherine Chan<sup>c</sup>, Alison Wenham<sup>c</sup>, Michael Stenbæk Schmidt<sup>a</sup>, Anja Boisen<sup>a</sup>, Ole Hansen<sup>a,b</sup>, Stuart Wenham<sup>c</sup>, Allen Barnett<sup>c</sup>

<sup>a</sup>*Department of Micro- and Nanotechnology, Technical University of Denmark (DTU)*

<sup>b</sup>*Danish National Research Foundation's Center for Individual Nanoparticle Functionality (CINF), Technical University of Denmark, DK-2800 Kgs.Lyngby, Denmark*

<sup>c</sup>*School of Photovoltaic and Renewable Energy Engineering, UNSW Australia, Sydney 2052, NSW, Australia*

---

## Abstract

We report fabrication of nanostructured, laser-doped selective emitter (LDSE) silicon solar cells with power conversion efficiency of 18.1 % and a fill factor (FF) of 80.1 %. The nanostructured solar cells were realized through a single step, mask-less, scalable reactive ion etch (RIE) texturing of the surface. The selective emitter was formed by means of laser doping using a continuous wave (CW) laser and subsequent contact formation using light-induced plating of Ni and Cu. The combination of RIE-texturing and a LDSE cell design has to our knowledge not been demonstrated previously. The resulting efficiency indicates a promising potential, especially considering that the cell reported in this work is the first proof-of-concept and that the fabricated cell is not fully optimized in terms of plating, emitter sheet resistance and surface passivation. Due to the scalable nature and simplicity of RIE-texturing as well as the LDSE process, we consider this specific combination a promising candidate for a cost-efficient process for future Si solar cells.

**Keywords:** black silicon, reactive ion etching, laser doping, LDSE, plating

---

---

\*Corresponding Author, email: [rasda@nanotech.dtu.dk](mailto:rasda@nanotech.dtu.dk), Ørsteds Plads building 345 East, 2800 Lyngby, Denmark, Tel.: +45 26187249

## 1. Introduction

Nanoscale texturing of silicon (Si) surfaces has been shown [1, 2, 3, 4, 5, 6, 7] to reduce the total weighted average optical reflectance to well below 1 % over a broad range of wavelengths and incident angles. Compared to the typical front surface reflectance of  $\sim 2$  and  $\sim 8$  %, from conventionally textured mono- [8] and multi-crystalline [9] Si solar cells, respectively, nanoscale texturing such as described in [10, 11, 12] offers a potential of improved power conversion efficiency for Si solar cells due to reduced reflectance loss.

We use black silicon [13, 14, 11] nanostructuring to achieve low reflectance, which can be modelled in a mean-field approximation as a graded refractive index at the Si-air interface [15]. von Gastrow *et al.* [16] reported excellent passivation of black Si surfaces using atomic layer deposition (ALD) of  $\text{Al}_2\text{O}_3$ . Repo *et al.* [17] achieved a power conversion efficiency of 18.7 % on 400  $\mu\text{m}$  thick float-zone Si using cryogenic deep reactive ion etching (RIE) as texturing and plasma assisted atomic layer deposition (ALD) of  $\text{Al}_2\text{O}_3$  for a passivated emitter rear locally diffused (PERL) cell and 22.1 % on an interdigitated back contact (IBC) cell with similar ALD-passivation [18]. Oh *et al.* [19] achieved a power conversion efficiency of 18.2 % on 300  $\mu\text{m}$  thick float-zone Si by combining a metal-assisted wet etching black silicon process for texturing, tetramethylammonium hydroxide (TMAH) damage removal etch and thermal  $\text{SiO}_2$  passivation. Yoo *et al.* [20] used industry grade Czochralski (Cz) Si and RIE texturing and achieved a power conversion efficiency of 16.7 %. Wang *et al.* [21] applied black Si by metal-assisted wet etching and ALD of  $\text{Al}_2\text{O}_3$  on industry grade Cz Si and achieved 18.2 % efficiency.

The primary reason for the relatively low efficiencies reported for black Si solar cells so far is the significant emitter and surface recombination [19, 2] resulting from increased surface area, defects from the texturing process and increased emitter doping through the nanostructured surface yielding increased Auger recombination. These effects usually lead to reduced short-circuit current and open-circuit voltage. Thus, a selective emitter design could improve the effi-

ciency of black Si solar cells. In order to achieve a selective emitter without the use of multiple high-temperature process steps and photolithography, laser doping and subsequent self-aligned Ni/Cu-plating has been suggested by several groups [22, 23, 24]. The laser-doped selective emitter (LDSE) process offers  
35 excellent sheet resistance control, self-alignment of front metal contacts to the local highly doped areas and a fast, low-temperature process scalable to industrial throughput. Hallam *et al.* achieved 19.3% efficiency for a LDSE solar cell on large-area Cz Si substrates using an industrial turnkey production line with the addition of laser-doping and plating [25]. The LDSE process has also been  
40 successfully applied to bifacial silicon solar cells [26]. An important feature of the LDSE cell process is the replacement of screen-printed Ag front contacts with plated Ni/Cu-contacts. Due to the economic benefits of replacing Ag by Cu in the solar industry [27] and the extensive studies of Ni/Cu-plating applied for Si solar cells [28, 29, 30, 31] the self-aligned, high-performing Ni/Cu-plated  
45 front contacts is an important and promising feature of LDSE solar cells.

This work presents LDSE black Si solar cells fabricated on p-type Cz Si substrates textured by a single step, maskless RIE process. To our knowledge this combination has not been previously reported and the resulting cell is thus considered a first proof-of-concept. The emitter diffusion and surface passivation  
50 were not fully optimized, since the main goal of this study was the combination of LDSE and RIE-texturing. The primary objective of this work is to investigate how laser doping and plating processes are affected by the RIE-textured surface and vice versa. It is not obvious how a differently textured surface affects e.g. electrical properties of the laser doped regions and subsequent plating.

55 The surface topology may alter the interaction between the laser beam and the material. Thus a different emitter profile may change the defect generation and risk of Schottky contact formation. Besides laser doping and plating, several process steps could be affected by changing from conventional to RIE-texturing: Emitter diffusion could change with effective surface area and deposition of anti-  
60 reflective coating may not yield the expected layer thickness and uniformity due to the nanostructured front surface. Such effects could then further affect the



subsequent laser doping and plating processes. An example hereof is spurious plating on the surface in case of pinholes in the dielectric coating resulting from the different surface topology.

65 For these reasons there is a need for an investigation of such RIE-textured LDSE solar cells.

## 2. Approach

The maskless RIE process presented in this work is applied as the texturing step in the following solar cell fabrication process:

- 70 • Saw damage removal by etching in 30 % KOH at 75 °C for 2 minutes and subsequent cleaning in 20 % HCl at room temperature for 5 minutes and rinsing in deionized water.
- Texturing using maskless RIE at room temperature in a O<sub>2</sub> and SF<sub>6</sub> plasma with a gas flow ratio of O<sub>2</sub>:SF<sub>6</sub> = 1:1, chamber pressure of 24  
75 mTorr, 13.56 MHz radio-frequency platen power of 100 W using a SPTS RIE system.
- Emitter formation using a tube furnace from Tempres Systems with liquid POCl<sub>3</sub> as dopant source at a temperature of 840 °C and atmospheric pressure for 50 min in O<sub>2</sub> and N<sub>2</sub> ambient, followed by removal of phosphor-silicate glass (PSG) in 5 % hydrofluoric acid (HF).  
80
- Plasma enhanced chemical vapour deposition (PECVD) of 75 nm hydrogenated amorphous silicon nitride (SiN<sub>x</sub>:H) anti-reflective coating at 400 °C using a Roth & Rau MAiA tool.
- Screen-printing of Al rear contact with standard Al paste, which was fired  
85 using a Sierra Therm infra-red fast-firing furnace, with a peak temperature set point of 835 °C and a belt speed of 4500 mm/min.

- Laser doping of the front surface using spin-on of 85 % phosphoric acid as doping source followed by laser doping using a continuous wave laser at a wavelength of 532 nm, 20 W laser power and 2-4 m/s laser scan speed.
- 90 • Light-induced plating of Ni acting as seed and barrier layer for the subsequent Cu plating
- Ni sintering using rapid thermal processing (RTP) in N<sub>2</sub> ambient at 350 °C for 2 minutes
- Light-induced plating of Cu onto the Ni seed layer
- 95 • Edge isolation by laser ablation using a 20 W Nd:YAG Lee laser tool.

The starting substrates were 25x25 mm<sup>2</sup> p-type, CZ mono-crystalline Si with a thickness of 200  $\mu$ m and a resistivity of 1-3  $\Omega$  cm.

Figure 1 shows a schematic cross-section of the fabricated solar cell.

### 100 3. Characterization

J-V curves and photovoltaic performance including short-circuit current density,  $J_{SC}$ , open-circuit voltage,  $V_{OC}$ , fill factor, FF, and power conversion efficiency were measured on complete cells under 1 sun illumination (1000 W/m<sup>2</sup>, AM1.5G) using a ELH halogen light source, Advantest TR6143 DC Source Measurement Unit and Labview software for data collection. The illumination was  
105 calibrated using the known short-circuit current of a reference mono-crystalline Si screen-printed solar cell.

A LEO 1550 Scanning Electron Microscope (SEM) was used to characterize the nanostructured surface topology.

110 Suns- $V_{OC}$  [32, 33] measurements were performed using a Sinton WCT-120 Lifetime tester. The  $J_{SC}$  value from the IV-measurement was used.

Reflectance was measured using a Perkin Elmer integrating sphere and spectrometer. The absorptance was measured using a center mount sample holder

inside the integrating sphere.

115 External Quantum Efficiency (EQE) was measured without bias light using a  
PV Measurement QE system and Internal Quantum Efficiency (IQE) was cal-  
culated based on the EQE and reflectance measurements.

Photoluminescence (PL) [34] was measured at open-circuit conditions using a  
BTi luminescence imaging tool.

120 Cross-sectional Focused Ion Beam (FIB)/SEM images of the plated Ni/Cu front  
contacts were taken using a Helios Nanolab 600 tool from FEI.

#### 4. Results

Figure 2 shows a SEM image of the RIE-textured Si surface at  $40^\circ$  tilt before  
any further processing. The nanostructures have a height of  $\sim 300$ - $500$  nm and  
125 a distance between the structures of  $\sim 300$ - $500$  nm. The nanostructures are  
conical-like hillocks randomly distributed across the entire solar cell surface.

Figure 3 shows the total light absorptance of the RIE-textured Si wafer before  
any further processing as function of wavelength. The absorptance was mea-  
sured using a centre-mount sample holder placed inside the integrating sphere.  
130 The incident angle of the light source deviated  $8^\circ$  from normal incidence due to  
the geometry of the measurement setup. The absorptance is  $\sim 99\%$  in most of  
the solar spectrum up to a wavelength of  $\sim 1000$  nm, at which the light starts to  
transmit through the  $200\ \mu\text{m}$  thick Si wafer. The integrated average absorptance  
is  $99.2\%$  in the wavelength range  $300$ - $900$  nm and decreases to  $91.7\%$  from  $900$   
135 to  $1000$  nm. The calculated absorptance of a  $200\ \mu\text{m}$  Si wafer without any tex-  
turing but with an assumed reflectance of  $0\%$  is plotted for comparison. Also,  
the simulated absorptance of a  $200\ \mu\text{m}$  Si wafer textured with upright random  
pyramids with  $75\ \text{nm}$   $\text{SiN}_x\text{:H}$  AR-coating is shown for comparison. It is seen  
that RIE-texturing results in increased absorptance of wavelengths above  $1000$   
140 nm compared to non-textured Si and similar absorptance of wavelengths above  
 $1000$  nm compared to conventionally textured mono-crystalline Si solar cells.  
This indicates some path-length enhancement of longer wavelengths within the

RIE-textured wafer. Based on the absorption coefficient of Si the path-length enhancement of RIE-textured Si is estimated to 20 times at a wavelength of 1100 nm.

The fabricated RIE-textured LDSE solar cells were characterized under 1 sun illumination ( $1000 \text{ W/m}^2$ , AM1.5G). Figure 4 shows the measured J-V curve of the best black Si LDSE cell at 1 sun. The short-circuit current density,  $J_{SC}$ , is  $36.3 \text{ mA/cm}^2$  and open-circuit voltage,  $V_{OC}$ , is 624 mV. The power conversion efficiency is 18.1 % and the fill factor, FF, is 80.1 %. The pseudo light J-V curve and Suns- $V_{OC}$  measurement seen in Figure 5 shows that the best black Si LDSE cell has a pseudo fill factor, pFF, of 82.3 % and a pseudo power conversion efficiency, pEff, of 18.7 % without the effect of series resistance. The high pFF indicates that shunting is low and the pseudo efficiency indicates that series resistance accounts for  $\sim 0.6$  % point efficiency loss compared to the actual power conversion efficiency. The linearly increasing relationship between the illumination and  $V_{OC}$  seen in the bottom part of Figure 5 indicates that neither shunting nor Schottky contacts are significant for the best black Si LDSE cell. This is encouraging considering the effect texturing may have on laser doping and plating processes, which could lead to increased defect generation. This does not seem to be the case from the Suns- $V_{OC}$  measurement. The increase in  $V_{OC}$  for intensities of 6-7 suns compared to the double diode model may be due to saturation of the surface recombination, which dominates the cell performance at 1 sun.

Table 1 shows measured  $J_{SC}$ ,  $V_{OC}$ , power conversion efficiency and FF for three different RIE-textured LDSE solar cells processed at three different laser speeds. The results in Table 1 show that the three RIE-textured LDSE solar cells have efficiencies in the range 17.5-18.1 %. The differences are primarily due to differences in FF. The different fill factors may be explained by the different laser speeds according to the result in Figure 6, which shows Suns- $V_{OC}$  at low injection for the three RIE-textured LDSE cells with different laser speeds. Figure 6 shows that a laser speed of 3 m/s leads to the highest open circuit voltage at low injection and an almost linear relationship between  $V_{OC}$  and illumination

intensity. The cell processed at a laser speed of 2 m/s has significantly lower  
175  $V_{OC}$  at low injection and a less linear relationship between  $V_{OC}$  and intensity.  
This is also reflected in the lower pFF of this particular sample.

After Ni/Cu-plating it was clear that significant spurious plating had occurred  
and that the surface had local scratches and pinholes through the dielectric, in  
which Ni and Cu has plated unintentionally. The top part of Figure 7 shows  
180 photographs of the finished cells where the plating defects are visible. The bot-  
tom part of Figure 7 shows a SEM-image of the RIE-textured surface of the  
final cells, where an example of the spuriously plated Ni/Cu is also visible. In  
order to investigate the lines defined by the laser, optical microscope images  
were taken. The top image in Figure 8 shows an optical microscope image of  
185 laser-doped lines on the RIE-textured Si surface. The image was taken at the  
point where a metal finger intersects the busbar. The laser-scribed lines are  
approximately 20  $\mu\text{m}$  wide with  $\sim 5 \mu\text{m}$  laser damage on each side of the lines.  
Note that each busbar consists of 10 separate lines about 20  $\mu\text{m}$  wide, spaced  
 $\sim 80 \mu\text{m}$  apart and metallized in the same light-induced plating process as the  
190 fingers. The middle image of Figure 8 shows an optical microscope image of  
the Ni/Cu-plated metal lines in this case from the busbar lines. It is seen that  
the plated contacts are between 18 and 28  $\mu\text{m}$  wide. The total contact fraction  
is  $\sim 2.5 \%$  of the total cell area assuming 23  $\mu\text{m}$  wide fingers. The bottom  
image in Figure 8 shows a top-view SEM-image of a Ni/Cu-plated line. In the  
195 SEM-image an example of spurious metal plating is also seen.

Figure 9 shows a SEM-image of the cross-section of a laser-doped line plated  
with Ni/Cu. The cross-section was defined by a Focused Ion Beam (FIB). The  
plated metal line is  $\sim 30 \mu\text{m}$  wide and  $\sim 10 \mu\text{m}$  in height. The layer on top of  
the Ni/Cu-line is Pt used solely for sample protection during FIB cutting. Note  
200 that the black silicon nanostructures can be seen on the sides of the laser-doped  
line. The nanostructures are not seen in the laser-doped region in the center of  
the plated Si region, since the Si in this region has been melted and re-solidified  
during the laser doping process.

Figure 10 shows EQE and IQE of the complete 18.1% cell and total reflectance

205 of the RIE-textured Si with  $\sim 75$  nm  $\text{SiN}_x\text{:H}$  anti-reflective (AR) coating, before any further processing. The IQE is calculated from the measured EQE and reflectance. The IQE plotted in Figure 10 might be underestimated, since the reflectance was measured on textured Si with AR-coating but without any metal, while the EQE was measured on the complete cell. The beam spot of the  
 210 light source of the EQE-measurement was placed between two metal fingers, but any metal present within the beam spot of the EQE-measurement will increase reflectance and thus decrease EQE and thereby the calculated IQE, since the reflectance on Figure 10 is measured without any metal on the surface. The low IQE for short wavelengths may be due to a too highly doped emitter resulting  
 215 in increased Auger recombination and may also be due to increased surface recombination at the nanostructured Si surface.

The measured short-circuit current density can be compared to the expected value calculated from the EQE and the solar spectrum to verify consistency in the measurements. Let  $E_\lambda(\lambda)$  be the solar spectral irradiance as a function  
 220 of wavelength  $\lambda$  according to AM1.5G and  $Q_{\text{ext}}(\lambda)$  the measured EQE. Then the spectral current density is  $J_\lambda(\lambda) = e\lambda E_\lambda(\lambda)Q_{\text{ext}}(\lambda)/(hc)$  since  $hc/\lambda$  is the photon energy and  $e$  the unit charge, while  $h$  is Planck's constant and  $c$  the vacuum speed of light. It follows that the expected short-circuit current density is

$$J_{\text{SC}} = \int_{\lambda_{\text{min}}}^{\lambda_{\text{max}}} \frac{e\lambda}{hc} E_\lambda(\lambda) Q_{\text{ext}}(\lambda) d\lambda. \quad (1)$$

225 A numerical integration using  $\lambda_{\text{min}} = 300$  nm and  $\lambda_{\text{max}} = 1200$  nm results in the expected short-circuit current density  $36.5$  mA/cm<sup>2</sup> which is in almost perfect agreement with the  $36.3$  mA/cm<sup>2</sup> that was measured.

Figure 11 shows the total reflectance of the RIE-textured surface with AR-coating before and after Ni/Cu-plating, respectively, as function of wavelength.  
 230 It is clear that after metal plating the reflectance of the complete cell increases significantly. However, the increase is presumably partly due to the spurious plating seen in Figure 7. The beam spot size of the light source was  $\sim 2$  cm in diameter and covered the majority of the cell area including the busbar and

metal fingers.

235 Figure 12 shows an open-circuit photoluminescence (PL) image of the 18.1 %  
cell after Ni plating and sintering. The PL-image shows increased recombination  
at the laser-doped, Ni-plated busbar and fingers, which is expected for Si-metal  
interfaces. Furthermore, circular points or agglomerations of lower PL-signal  
intensity can be seen all over the surface. This indicates that the firing temper-  
240 ature used after rear Al screen-printing was slightly too high for the particular  
samples, leading to a non-uniform back-surface field.

## 5. Discussion

The power conversion efficiency of 18.1 % of the black Si LDSE cell fabricated  
245 in this work is comparable to the best efficiencies reported for front-contacted  
black Si solar cells [17, 19, 21]. Table 2 shows selected cell results reported for  
black Si solar cells [11]. From Table 2 it appears that the cell in this work has  
superior fill factor compared to existing black silicon cells, while  $J_{SC}$  and  $V_{OC}$   
are on par or slightly reduced compared to [17]. The lack of improvement to  $J_{SC}$   
250 and  $V_{OC}$  may be explained by the unintentionally too heavily doped emitter, in-  
adequate surface passivation and the unintentional spurious plating; optimized  
processing is thus expected to improve both key parameters significantly. The  
very high fill factor on the other hand is due to a near optimum laser power  
and scan speed used during laser doping of the best device, resulting in very  
255 low contact resistance. We note that the optimum laser doping conditions are  
different from those on planar silicon probably due to stronger coupling of the  
laser power into the structure.

In general, this result is encouraging considering that industrial grade Cz Si  
wafers were used and that the complete cells in this work were not fully opti-  
260 mized:

First of all the cells had significant spurious plating as shown in Figure 7. This  
induces a direct loss of current, since the reflectance of the complete cells is

significantly higher than a similar cell without spurious plating. The reflectance difference is shown in Figure 11 and the additional integrated average reflectance in the range 300-1000 nm attributed only to spurious plating can be estimated by the following considerations: The integrated average reflectance in the range 300-1000 nm is 1.20 % before plating and 6.38 % after plating. The front contact grid only covers  $\sim 2.5$  % of the cell area assuming 23  $\mu\text{m}$  wide fingers. Based on the metal grid coverage the grid itself only accounts for additional reflectance of  $\sim 1.23$  % assuming 50 % reflectance of Cu in the wavelength range 300-1000 nm. The spurious plating must account for the difference between the additional reflectance after plating and reflectance from the grid. Thus the spurious plating accounts for  $\sim 3.95$  %. This is a direct reflection loss, which can be at least partly avoided by minimizing spurious plating. Furthermore, spurious plating in scratches such as seen in Figure 7 is likely to cause increased surface recombination, since the plated metal contacts directly to a lightly doped emitter, which shields minority carriers less than a heavily doped emitter, thus causing enhanced recombination at the metal-Si interface. It is however encouraging that the Suns- $V_{\text{OC}}$  measurement in Figure 5 does not indicate any increased defect generation or Schottky contact formation.

The Suns- $V_{\text{OC}}$  result in Figure 6 indicates the relationship between laser speed and pseudo FF. From the result in Figure 6 it seems that 3 m/s leads to the most ideal performance, ultimately leading to a higher FF and power conversion efficiency than the cells processed at 2 and 4 m/s, respectively. The lower  $V_{\text{OC}}$  at low injection for the cell processed at 2 m/s may be due to increased laser damage at the slower scan speed leading to increased Shockley-Read-Hall recombination in the laser doped regions. The pseudo FF of the cell processed at 4 m/s is almost as high as for 3 m/s. However, the FF is still significantly lower, which indicates that the problem for this cell is rather series resistance. This may be due to a lighter doping caused by the faster scan speed. Thus, it seems that a laser speed of 3 m/s is close to the optimal compromise between minimized laser damage and minimized series resistance for RIE-textured laser-doped solar cells.



Assuming that the spurious plating is due to pinholes and other non-uniformities  
 295 in the dielectric AR-coating, the problem could be minimized by increasing the  
 thickness of the  $\text{SiN}_x\text{:H}$  layer. The layer may be even thinner than expected,  
 because the deposition rate in the PECVD process may not be the same for  
 RIE-textured Si compared to conventionally textured Si. Even a non-uniform  
 layer would not induce spurious plating as long as the dielectric layer is com-  
 300 pletely covering the Si surface with sufficient thickness to completely isolate the  
 surface from the plating electrolyte. It is assumed that the pretreatment using  
 hydrofluoric acid (HF) immediately prior to Ni plating further increases the  
 risk of pinholes, since the  $\text{SiN}_x\text{:H}$  coating is etched by HF to some degree. A  
 negative effect of increasing the  $\text{SiN}_x\text{:H}$  thickness could be increased reflectance  
 305 and absorption in the AR-coating. However, the AR-properties of the  $\text{SiN}_x\text{:H}$   
 coating are less critical on RIE-textured Si, due to the very low reflectance from  
 the black Si surface itself. The increased absorption in the AR-coating could  
 be minimized by adjusting the layer thickness and the HF process in order to  
 minimize pinholes, while maintaining an acceptably low absorption in the AR-  
 310 coating.

The phosphorus emitter was too heavily doped resulting in a sheet resistance of  
 40  $\Omega$  measured with a 4-point probe after phosphorus diffusion. This was un-  
 intentional, since the full area sheet resistance of such selective emitter should  
 ideally be on the order of 100  $\Omega$ , which was also measured on planar Si reference  
 315 wafers from the same diffusion process. This suggests that the decreased sheet  
 resistance is due to faster diffusion of dopant atoms through the nanostructured  
 Si surface. By decreasing time and temperature of the diffusion process, we ex-  
 pect to improve the emitter in future studies. From the QE measurement seen  
 in Figure 10 a significant decrease in EQE and IQE is seen for wavelengths below  
 320 600 nm. This indicates significant emitter and surface recombination, which is  
 expected from black Si, if the surface is not well passivated. Since a standard  
 $\text{SiN}_x\text{:H}$  AR-coating was used as the only passivation layer on these cells, it is  
 expected that the short wavelength response can be significantly improved in  
 future studies by optimizing the  $\text{SiN}_x\text{:H}$  coating or by applying different dielec-

325 tric coatings.

From the PL-image in Figure 12 small circular structures with slightly lower PL-signal can be seen. We suggest that this is due to a too high firing temperature used for rear Al screen-printing on these particular samples. We expect this to be improved in future studies.

330 By combining the potential improvements mentioned above significantly higher power conversion efficiency of this new kind of cell structure is expected. This will be investigated in future studies.

## 6. Conclusion

Ni/Cu-plated black Si LDSE solar cells have been fabricated on industrial  
335 grade Cz Si substrates textured in a single step, maskless RIE-process. The best cell has a power conversion efficiency of 18.1 % with a fill factor of 80.1 %. Since the cell was not optimized in terms of spurious plating, emitter sheet resistance and surface passivation, it is expected that the efficiency of black Si LDSE cells will be significantly higher in the near future. To our knowledge this  
340 is the first RIE-textured LDSE cell reported and we therefore consider this a proof-of-concept.

## 7. Acknowledgements

The funding support for this work from the Australian Renewable Energy Agency (ARENA) is gratefully acknowledged. Center for Individual Nanoparticle  
345 Functionality (CINF) is sponsored by The Danish National Research Foundation (DNRF 54). The authors would like to thank Mattias Juhl for assistance with absorptance measurements. The authors would also like to thank Brett Hallam, Malcolm Abbott and Craig Johnson for advice on process flow and cell design.

## 350 8. References

- [1] Priolo, F., Gregorkiewicz, T., Galli, M., Krauss, T.F., Silicon nanostructures for photonics and photovoltaics, *Nature Nanotechnology* **9** 19-32 (2014) DOI: 10.1038/NNANO.2013.271.
- [2] Davidsen, R.S., Nordseth, Ø., Boisen, A., Schmidt, M.S., Hansen, O.,  
355 "Plasma texturing on large-area industrial grade CZ silicon solar cells",  
28th EU PVSEC Conference Proceedings (2013).
- [3] Zhu, J., Yu, Z., Fan, S., Cui, Y., "Nanostructured photon management for high performance solar cells", *Materials Science and Engineering R* **70** 330340 (2010)
- [4] Nguyen, K.N., Abi-Saab, D., Basset, P., Richalot, E., Marty, F., Angelescu, D., Leprince-Wang, Y., Bourouina, T., "Black silicon with sub-percent reflectivity: Influence of the 3D texturization geometry", *Solid-State Sensors, Actuators and Microsystems Conference (Transducers)*, 16th International Transducers **11** 354-357 (2011).  
360
- [5] Kelzenberg, M.D., Boettcher, S.W., Petykiewicz, J.A., Turner-Evans, D.B., Putnam, M.C., Warren, E.L., Spurgeon, J.M., Briggs, R.M., Lewis, N.S., Atwater, H.A., "Enhanced absorption and carrier collection in Si wire arrays for photovoltaic applications", *Nature Materials* **9** 239244 (2010), DOI: 10.1038/NMAT2635.  
365
- [6] Huang, Y-F., Chattopadhyay, S., Jen, Y-J., Peng, C-Y., Liu, T-A., Hsu, Y-K., Pan, C-L., Lo, H-C., Hsu, C-H., Chang, Y-H., Lee, C-S., Chen, K-H., Chen, L-C., "Improved broadband and quasiomnidirectional anti-reflection properties with biomimetic silicon nanostructures", *Nature Nanotechnology* **2** 770 - 774 (2007).  
370
- [7] Parretta, A., Sarno, A., Tortora, P., Yakubu, H., Maddalena, P., Zhao, J., Wang, A., "Angle-dependent reflectance measurements on photovoltaic materials and solar cells", *Optics Communications* **172** 139-151 (1999).  
375

- [8] Zhao, L., Zuo, Y.H., Zhou, C.L., Li, H.L., Diao, H.W., Wang, W.J., "Theoretical investigation on the absorption enhancement of the crystalline silicon solar cells by pyramid texture coated with SiNx:H layer", Solar Energy **85** 530-537 (2011).
- [9] Macdonald, D., Cuevas, A., Kerr, M., Samundsett, C., Ruby, D., Winderbaum, S., Leo, A., "Texturing Industrial Multicrystalline Silicon Solar Cells", Solar Energy **76** No.1 277-283 (2004)
- [10] Rahman, A., Ashraf, A., Xin, H., Tong, X., Sutter, P., Eisaman, M.D., Black, C.T., "Sub-50-nm self-assembled nanotextures for enhanced broadband antireflection in silicon solar cells", Nature Communications **6**, 5963 (2015), DOI: 10.1038/ncomms6963.
- [11] Liu, X., Coxon, P.R., Peters, M., Hoex, B., Cole, J.M., Fray, D.J., "Black Silicon: Fabrication methods, properties, and solar energy applications", Review Article, Energy & Environmental Science, Royal Society of Chemistry **7** 3223-3263 (2014) DOI: 10.1039/c4ee01152j.
- [12] Allen, T., Bullock, J., Cuevas, A., Baker-Finch, S., Karouta, F. "Reactive ion etched black silicon texturing: A comparative study", In Photovoltaic Specialist Conference (PVSC), IEEE **40th**, pp. 0562-0566, IEEE (2014), doi:10.1109/PVSC.2014.6924983
- [13] Her, T.H., Finlay, R.J., Wu, C., Deliwala, S., Mazur, E., "Microstructuring of silicon with femtosecond laser pulses", Appl. Phys. Lett. **73** 1673-1675 (1998).
- [14] Jansen, H., Deboer, M., Legtenberg, R., Elwenspoek, M., "The Black Silicon Method - a Universal Method for Determining the Parameter Setting of a Fluorine-Based Reactive Ion Etcher in Deep Silicon Trench Etching with Profile Control", Journal of Micromechanics and Microengineering **5** 115-120 (1995).

- 405 [15] Stephens, R.B., Cody, G.D., "Optical Reflectance and Transmission of a Textured Surface", *Thin Solid Films* **45** 19-29 (1977).
- [16] von Gastrow, G., Alcubilla, R., Ortega, P., Yli-Koski, M., Conesa-Boj, S., i Morral, A. F., Savin, H., "Analysis of the Atomic Layer Deposited Al<sub>2</sub>O<sub>3</sub> field-effect passivation in black silicon", *Solar Energy Materials and Solar*  
410 *Cells* **142**, 29-33 (2015), doi:10.1016/j.solmat.2015.05.027
- [17] Repo, P., Benick, J., Vähänissi, V., Schön, J., von Gastrow, G., Steinhäuser, B., Schubert, M.C., Hermle, M., Savin, H., "N-type black silicon solar cells", *SiliconPV, Energy Procedia* **38** 866-871 (2013).
- [18] Savin, H., Repo, P., von Gastrow, G., Ortega, P., Calle, E., Garn, M.,  
415 Alcubilla, R., "Black silicon solar cells with interdigitated back-contacts achieve 22.1% efficiency", *Nature nanotechnology* **10** 624628 (2015), doi: 10.1038/NNANO.2015.89
- [19] Oh, J., Yuan, H.C., Branz, H., "An 18.2 %-efficient black-silicon solar cell achieved through control of carrier recombination in nanostructures",  
420 *Nature Nanotechnology* **7** 743-748 (2012).
- [20] Yoo, J., "Reactive ion etching (RIE) technique for application in crystalline silicon solar cells", *Solar Energy* **84** 730-734 (2010).
- [21] Wang, W-C., Lin, C-W., Chen, H-J., Chang, C-W., Huang, J-J., Yang, M-J., Tjahjono, B., Huang, J-J., Hsu, W-C., Chen, M-J., "Surface Passivation of Efficient Nanotextured Black Silicon Solar Cells Using Thermal Atomic  
425 Layer Deposition", *ACS Appl. Mater. Interfaces* **5** 97529759 (2013) DOI: dx.doi.org/10.1021/am402889k
- [22] Kyeong, D., Cho, S-H., Lim, J-K., Lee, K., Hwang, M-I., Lee, W-J., Cho, E.C., "Approaching 20%-efficient selective-emitter solar cells with copper  
430 front contacts on industrial 156 mm CZ Si wafers", *Proceedings, 27th European Photovoltaic Solar Energy Conference and Exhibition* (2012)

- [23] Hallam, B., Uruea, A., Russell, R., Aleman, M., Abbott, M., Dang, C., Wenham, S., Tous, L., Poortmans, J., "Efficiency enhancement of i-PERC solar cells by implementation of a laser doped selective emitter", Solar Energy Materials & Solar Cells **134** 89-98 (2015)
- [24] Tousa, L., Russella, R., Dasa, J., Labiea, R., Ngamoc, M., Horzela, J., Philipsena, H., Sniekersb, J., Vandermissena, K., van den Brekeld, L., Janssensena, T., Alemana, M., van Dorpa, D.H., Poortmansa, J., Mertens, R., "Large area copper plated silicon solar cell exceeding 19.5% efficiency", 3rd Workshop on Metallization for Crystalline Silicon Solar cells (2011)
- [25] Hallam, B., Wenham, S., Sugianto, A., Mai, L., Chong, C., Edwards, M., Jordan, D., Fath, P., "Record Large-Area p-Type CZ Production Cell Efficiency of 19.3% Based on LDSE Technology", IEEE Journal of Photovoltaics **1** No. 1 43-48 (2011)
- [26] Wang, X., Allen, V., Vais, V., Zhao, Y., Tjahjono, B., Yao, Y., Wenham, S., Lennon, A., "Laser-doped metal-plated bifacial silicon solar cells", Solar Energy Materials & Solar Cells **131** 37-45 (2014)
- [27] Green, M.A., "Silicon solar cells: State-of-the-art", Phil. Trans. R. Soc. A **371** (2013), DOI: [dx.doi.org/10.1098/rsta.2011.0413](https://doi.org/10.1098/rsta.2011.0413)
- [28] Flynn, S., Lennon, A., "Copper penetration in laser-doped selective-emitter silicon solar cells with plated nickel barrier layers", Solar Energy Materials & Solar Cells **130** 309316 (2014)
- [29] Rehman, A.u., Lee, S.H., "Review of the Potential of the Ni/Cu Plating Technique for Crystalline Silicon Solar Cells", Materials **7** 1318-1341 (2014), DOI:10.3390/ma7021318
- [30] Geisler, C., Hördt, W., Kluska, S., Mondon, A., Hopman, S., Glatthaar, M., "Overcoming electrical and mechanical challenges of continuous wave laser processing for NiCu plated solar cells", Solar Energy Materials & Solar Cells **133** 4855 (2015)

- 460 [31] Su Zhou, Chunlan Zhou, Wenjing Wang, Junjie Zhu, Yehua Tang, Jingwei  
Chen, Yan Zhao, "Comprehensive study of light induced plating of nickel  
and its effect on large area laser doped crystalline solar cells" Solar Energy  
Materials & Solar Cells **125** 3338 (2014)
- [32] Sinton, R. A., A. Cuevas, "A quasi-steady-state open-circuit voltage  
465 method for solar cell characterization" 16th European Photovoltaic Solar  
Energy Conference **25** 1152-1155 (2000).
- [33] Trupke, T., Bardos, R. A., Abbott, M. D., Cotter, J. E., "Suns-  
photoluminescence: Contactless determination of current-voltage charac-  
teristics of silicon wafers" Applied Physics Letters, **87** 9, 093503 (2005)
- 470 [34] Trupke, T., Bardos, R. A., Schubert, M. C., Warta, W. "Photoluminescence  
imaging of silicon wafers", Applied Physics Letters, **89** 4, 044107 (2006)

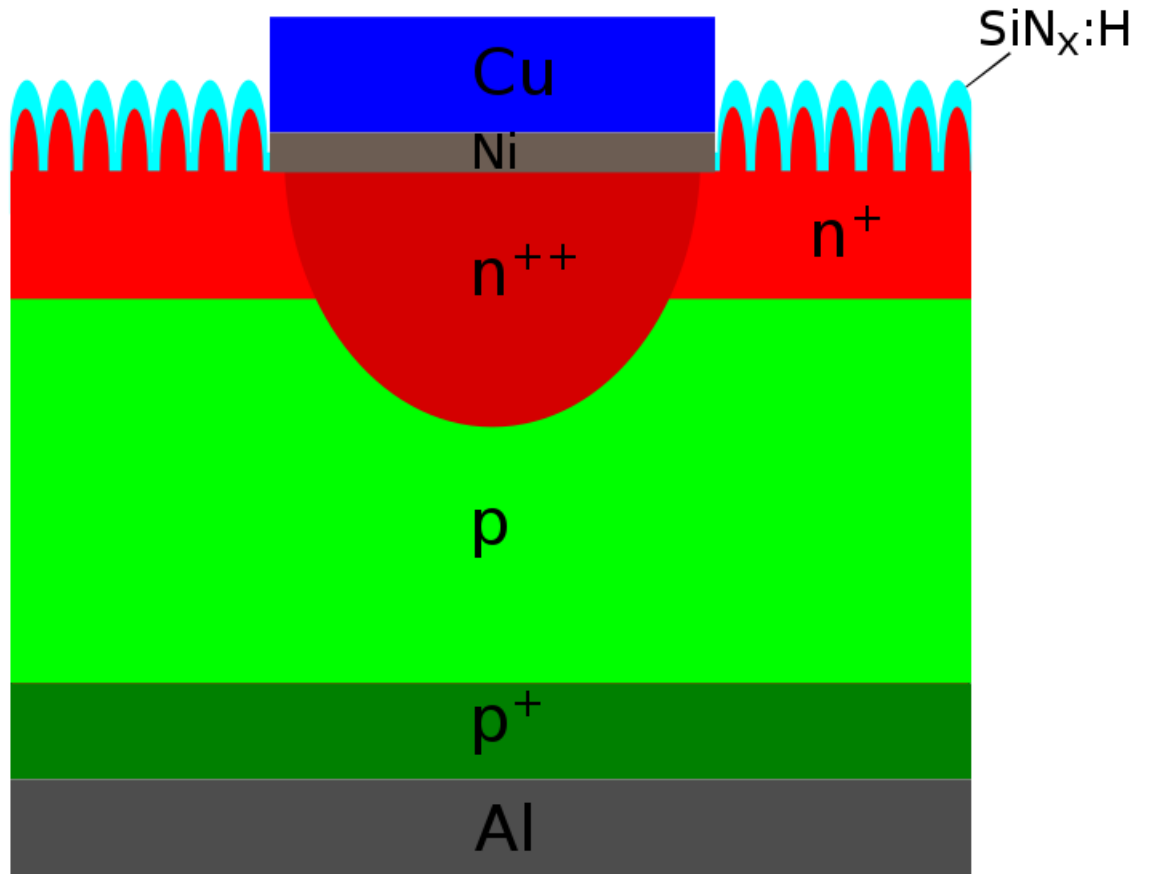


Figure 1: Sketch of the black Si LDSE solar cell structure. The cells are textured in a single-step, maskless RIE process. The highly doped regions of the selective emitter is formed by means of local laser doping using phosphoric acid dopant and a continuous wave laser. The rear contact is screen-printed and fired Al and the front contacts are plated Ni/Cu. The dimensions of the different layers are not to scale.



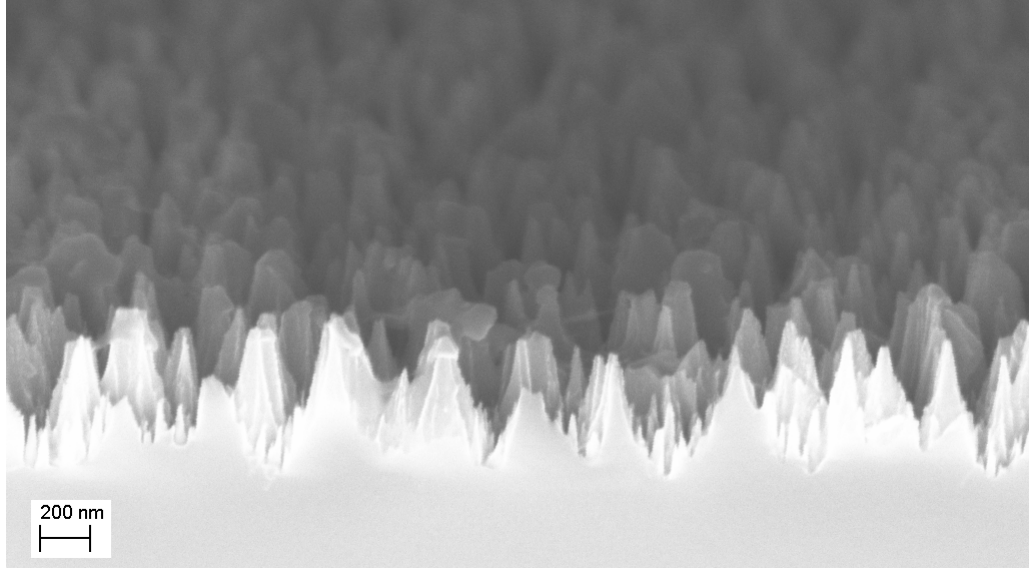


Figure 2: SEM-image at 40° tilt of the RIE-textured Si surface before any further processing. The nanostructures have a height of  $\sim 300\text{-}500$  nm and a distance between the structures of  $\sim 300\text{-}500$  nm. The nanostructures are conical-like hillocks randomly distributed across the entire solar cell surface.

Laser Speed	Efficiency [%]	$J_{SC}$ [mA/cm <sup>2</sup> ]	$V_{OC}$ [V]	FF [%]	pFF [%]
2m/s	17.5	36.0	0.624	77.9	81.0
3m/s	18.1	36.3	0.624	80.1	82.3
4m/s	17.5	35.8	0.624	78.4	82.0

Table 1: Power conversion efficiency, short-circuit current density, open-circuit voltage and fill factor at 1 sun illumination (1000 W/m<sup>2</sup>, AM1.5G) of conventionally and RIE-textured LDSE Si cells with laser speeds of 2, 3 and 4 m/s, respectively. Furthermore, the pseudo fill factor, pFF, determined by Suns- $V_{OC}$  measurements is given.

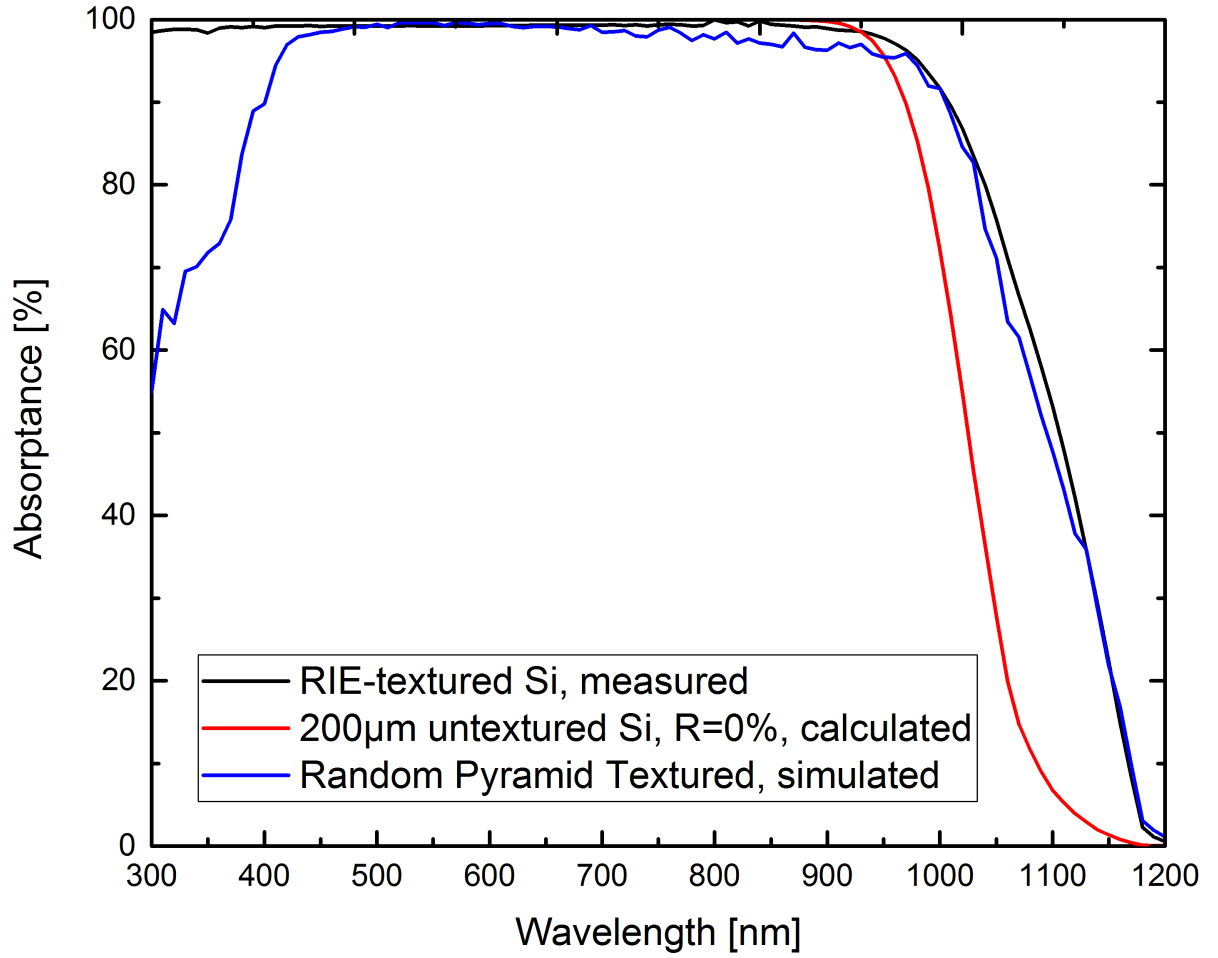


Figure 3: Light absorptance of the black Si surface before cell processing as function of the wavelength. The absorptance was measured with a center-mount inside an integrating sphere. The incident angle of the light source deviated  $8^\circ$  from normal incidence due to the geometry of the measurement setup.

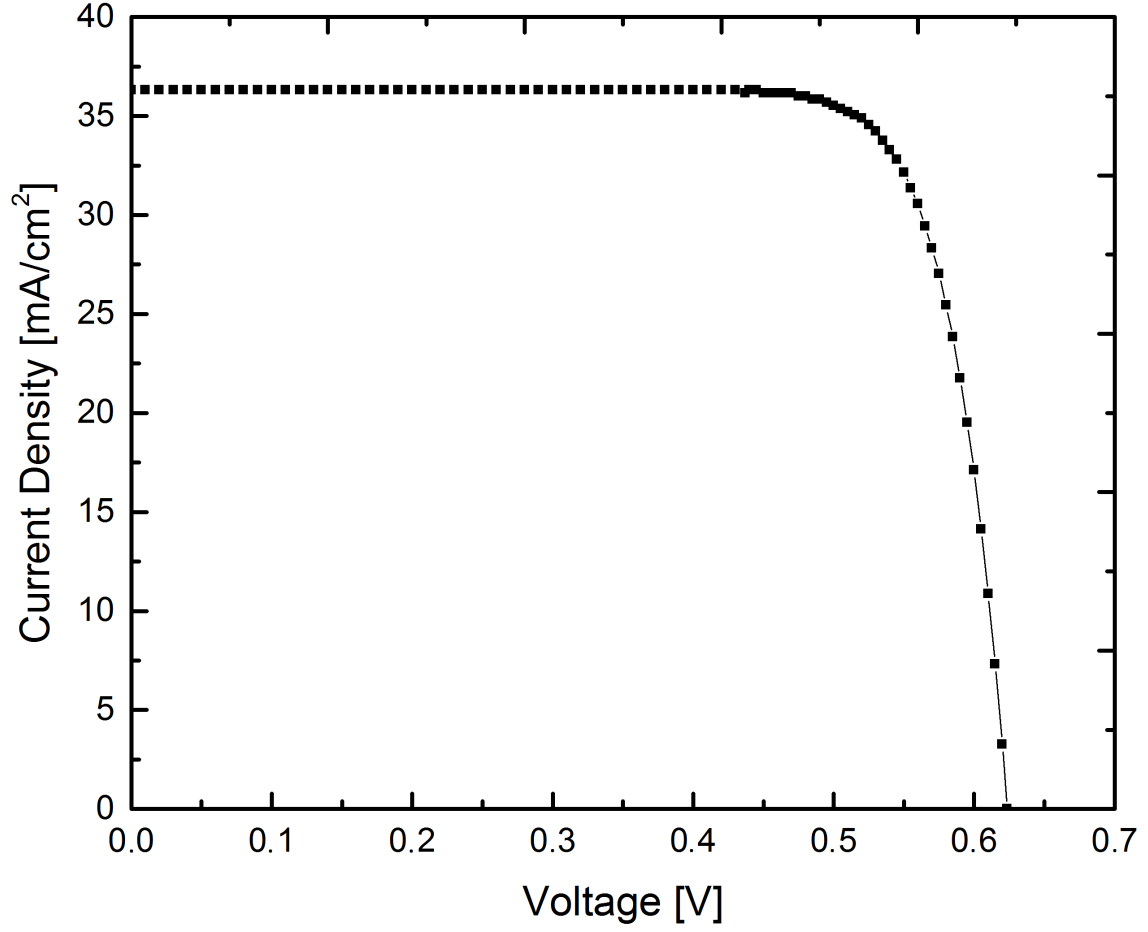
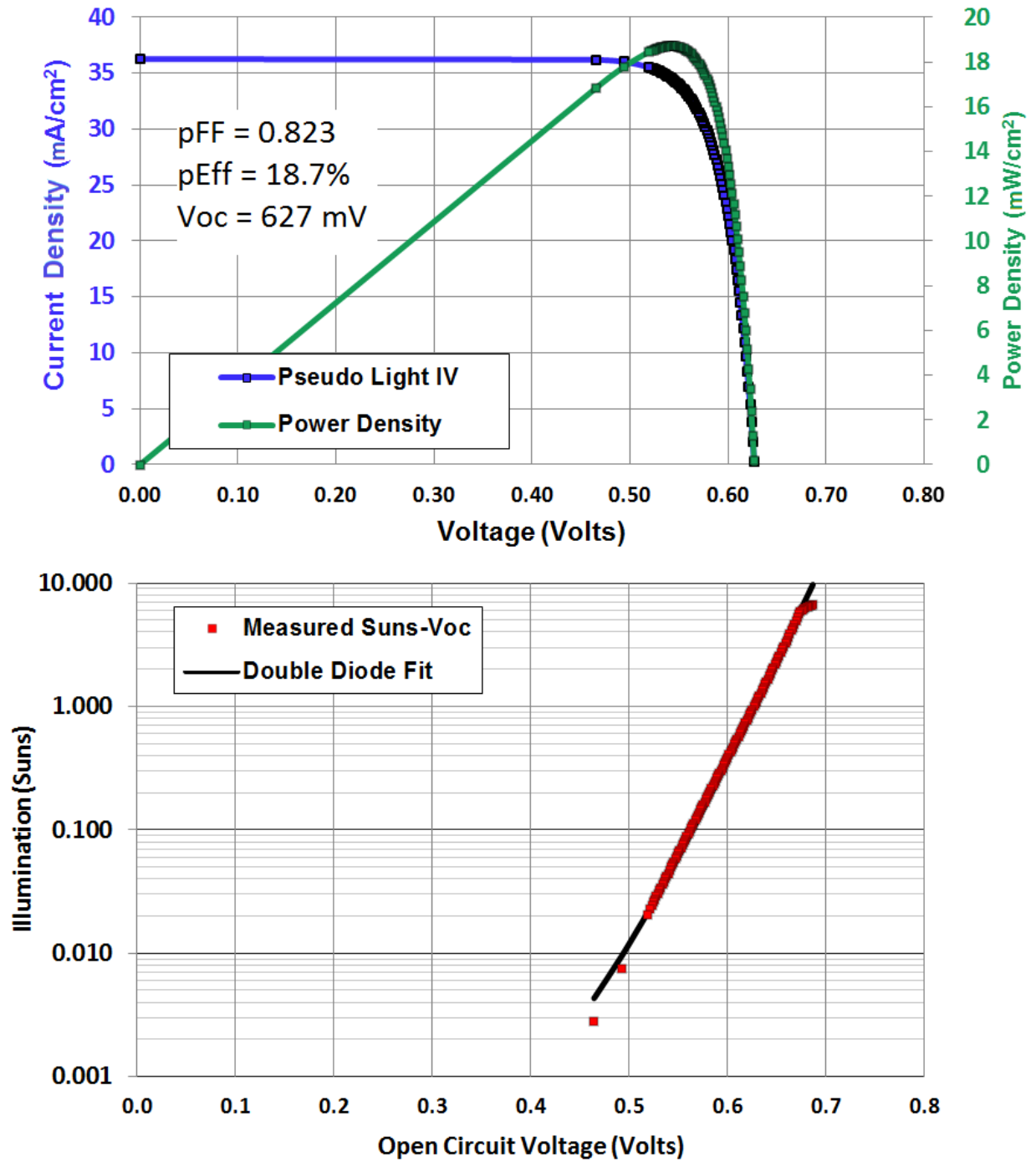


Figure 4: Current density-voltage characteristic of the best black Si LDSE solar cell under 1 sun illumination ( $1000 \text{ W/m}^2$ , AM1.5G). The short-circuit current density,  $J_{SC}$ , is  $36.3 \text{ mA/cm}^2$  and open-circuit voltage,  $V_{OC}$ , is  $624 \text{ mV}$ . The power conversion efficiency is  $18.1 \%$  and the fill factor, FF, is  $80.1 \%$



23  
 Figure 5: Result of the Pseudo Light J-V (top) and (middle) Suns- $V_{OC}$  measurement of the best black Si LDSE cell processed at a laser speed of 3 m/s. The measurement shows a pseudo fill factor, pFF, of 82.3 % and a pseudo efficiency, pEff, of 18.7 % without the effect of series resistance.

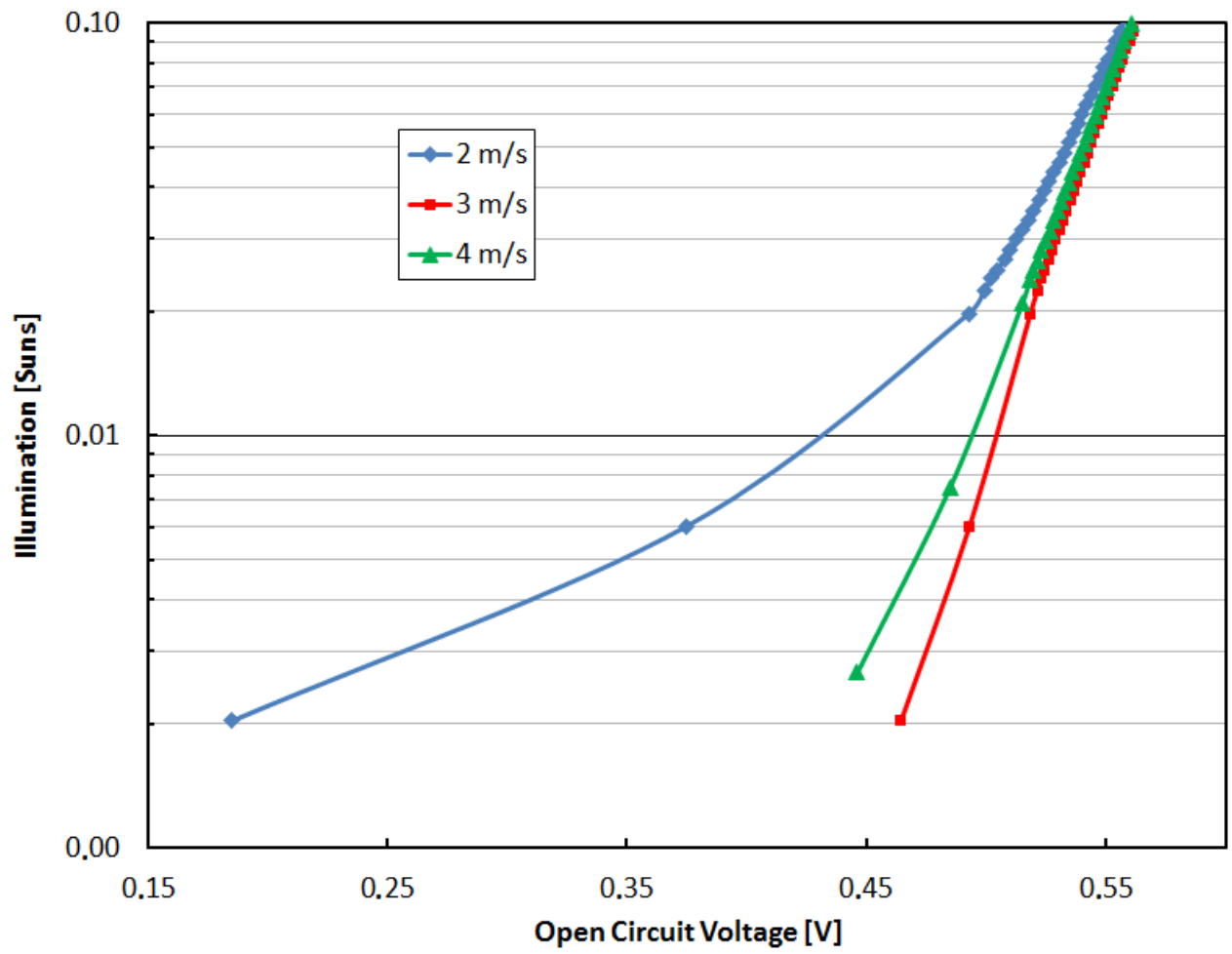


Figure 6: Suns- $V_{OC}$  measurement at low injection of three black Si LDSE cells processed at laser speeds of 2, 3 and 4 m/s, respectively.

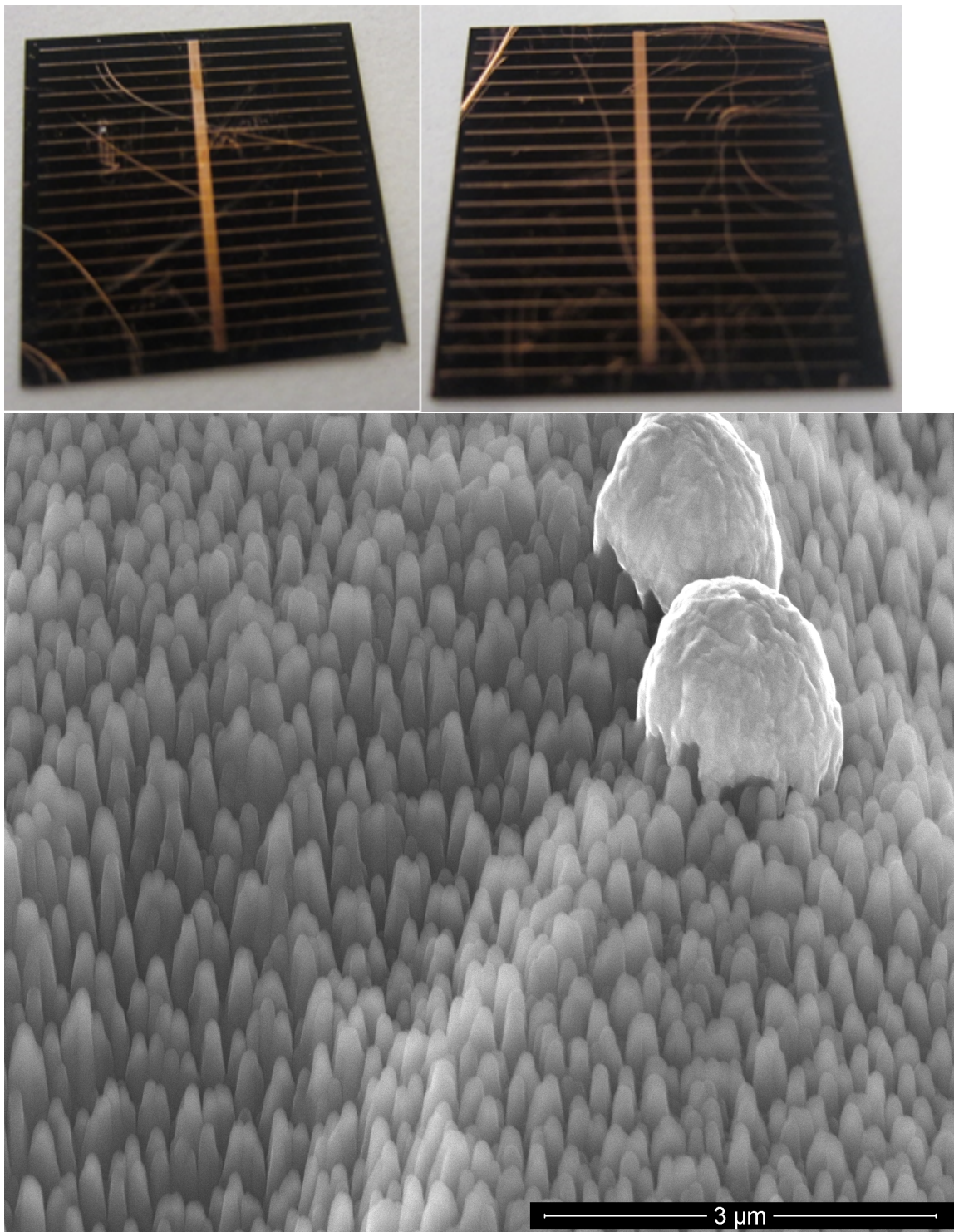


Figure 7: (Top) Photographs of 2 of the final black Si LDSE solar cells. The images show significant spurious plating of Ni/Cu and scratches in the front surface. (Bottom) SEM-image at 52° tilt of the RIE-textured surface of the final black Si LDSE solar cell surface. The SEM-image also shows examples of spuriously plated Ni/Cu.



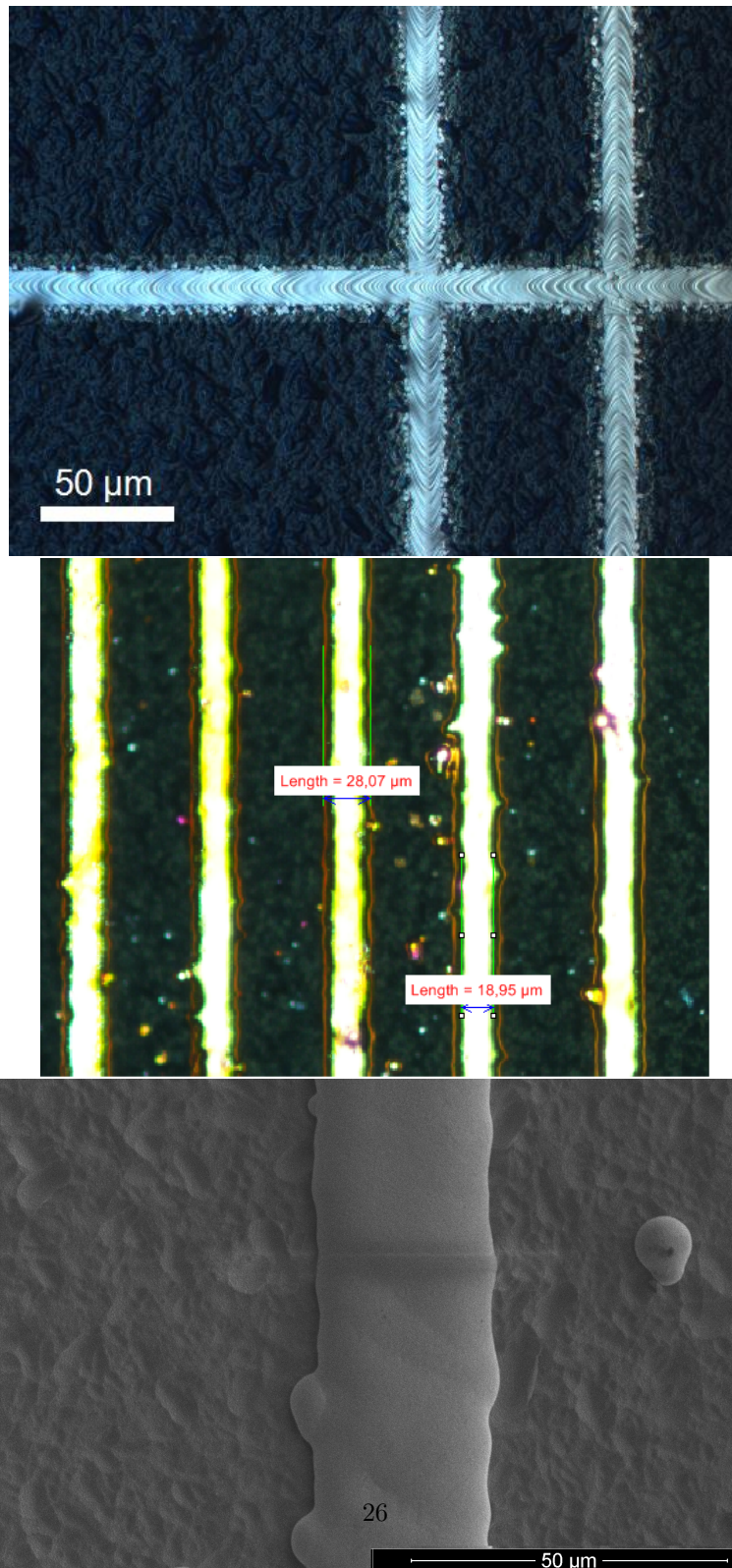


Figure 8: (Top) Optical microscope image of the laser-doped lines on the black Si front surface before Ni/Cu-plating. (Middle) Optical microscope image showing the width of the Ni/Cu-plated metal lines in this case from the busbar. (Bottom) Top-view SEM-image of a Ni/Cu-plated metal line.

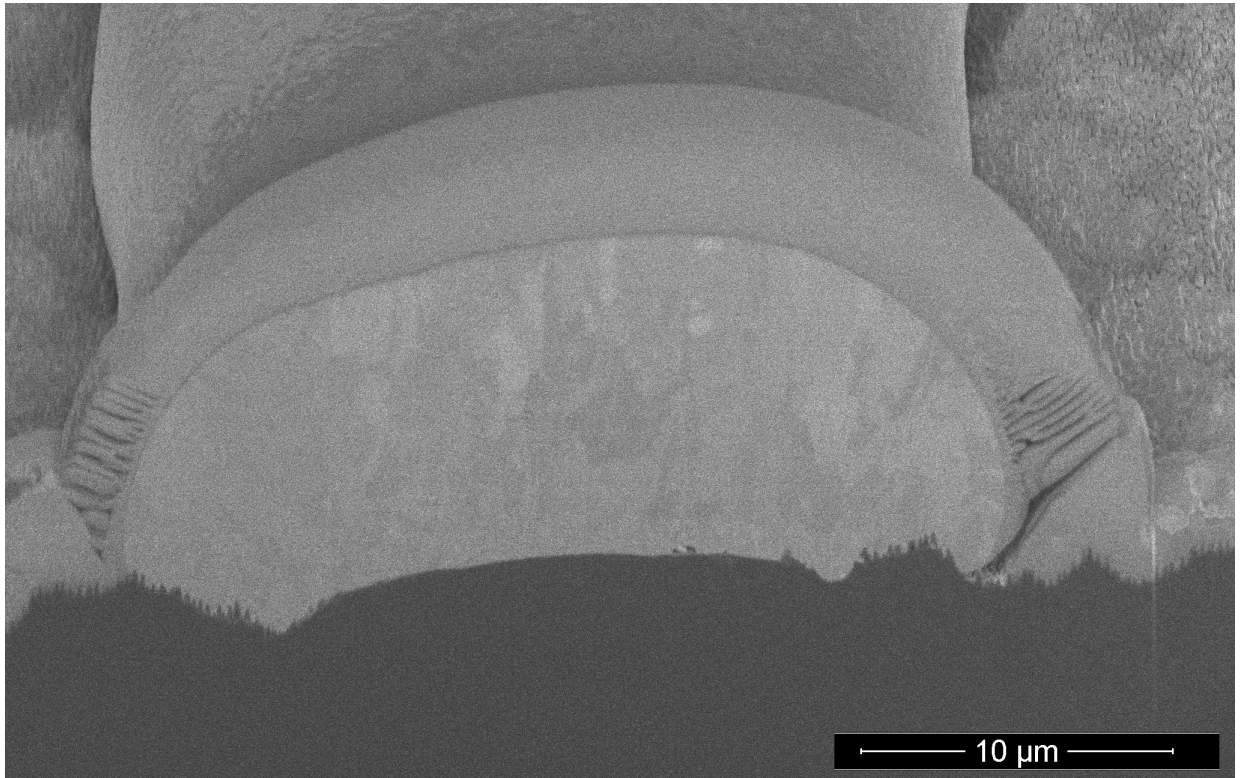


Figure 9: SEM-image at  $52^\circ$  tilt showing the cross-section of a Ni/Cu-plated metal line. The cross-section was defined by a Focused Ion Beam (FIB). The plated metal line is  $\sim 30\ \mu\text{m}$  wide and  $\sim 10\ \mu\text{m}$  in height. The layer seen on top of the Ni/Cu-line is Pt used solely for sample protection during FIB cutting. Note that the black silicon nanostructures are visible at the edges of the plated Ni/Cu line.



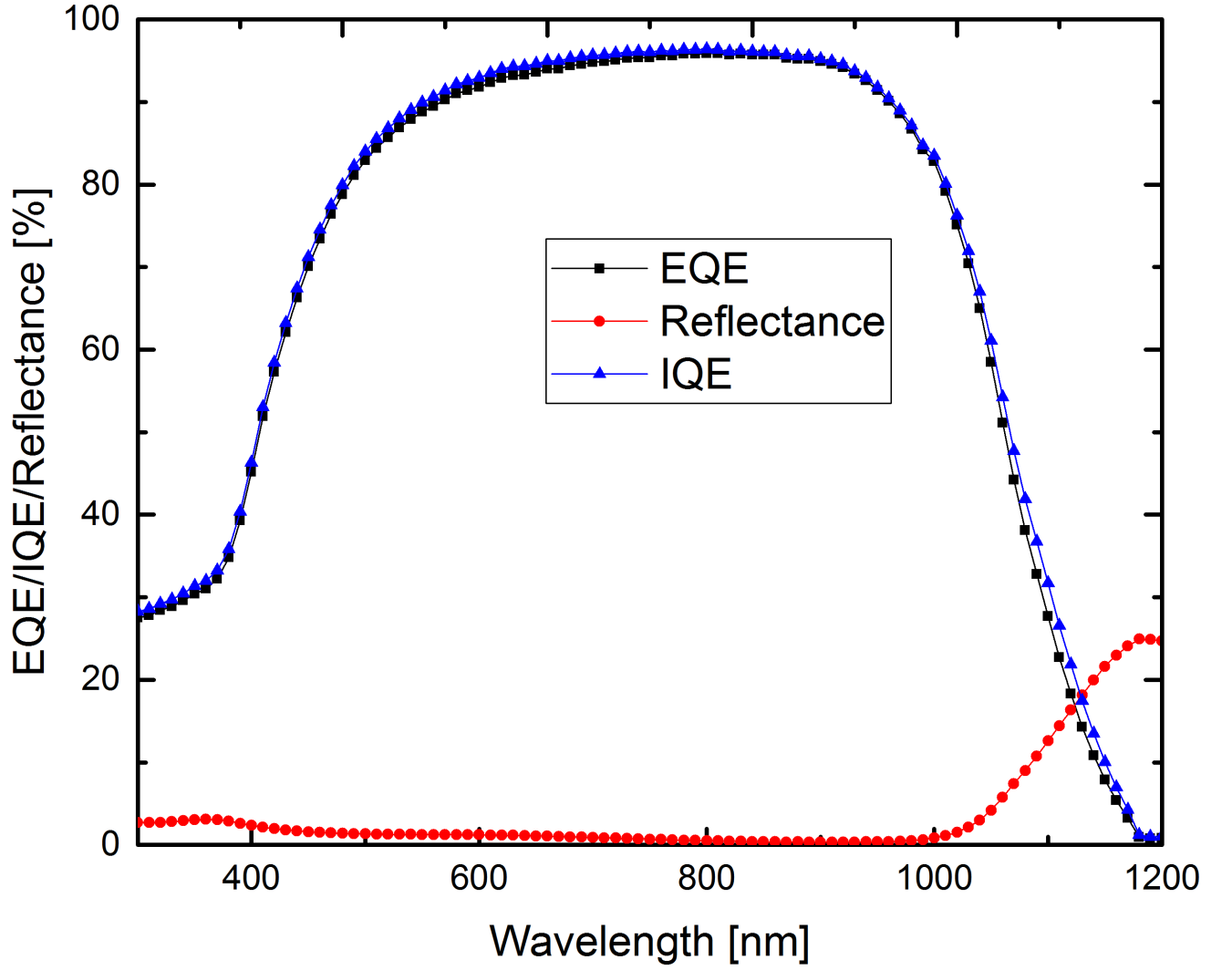


Figure 10: External and Internal Quantum Efficiency and total reflectance as function of wavelength of the 18.1% black Si LDSE solar cell. The reflectance data are for RIE-textured Si with AR-coating before any further processing. The IQE is calculated based on the measured EQE and reflectance of the surface measured before laser and plating processes. EQE was measured without any bias light.

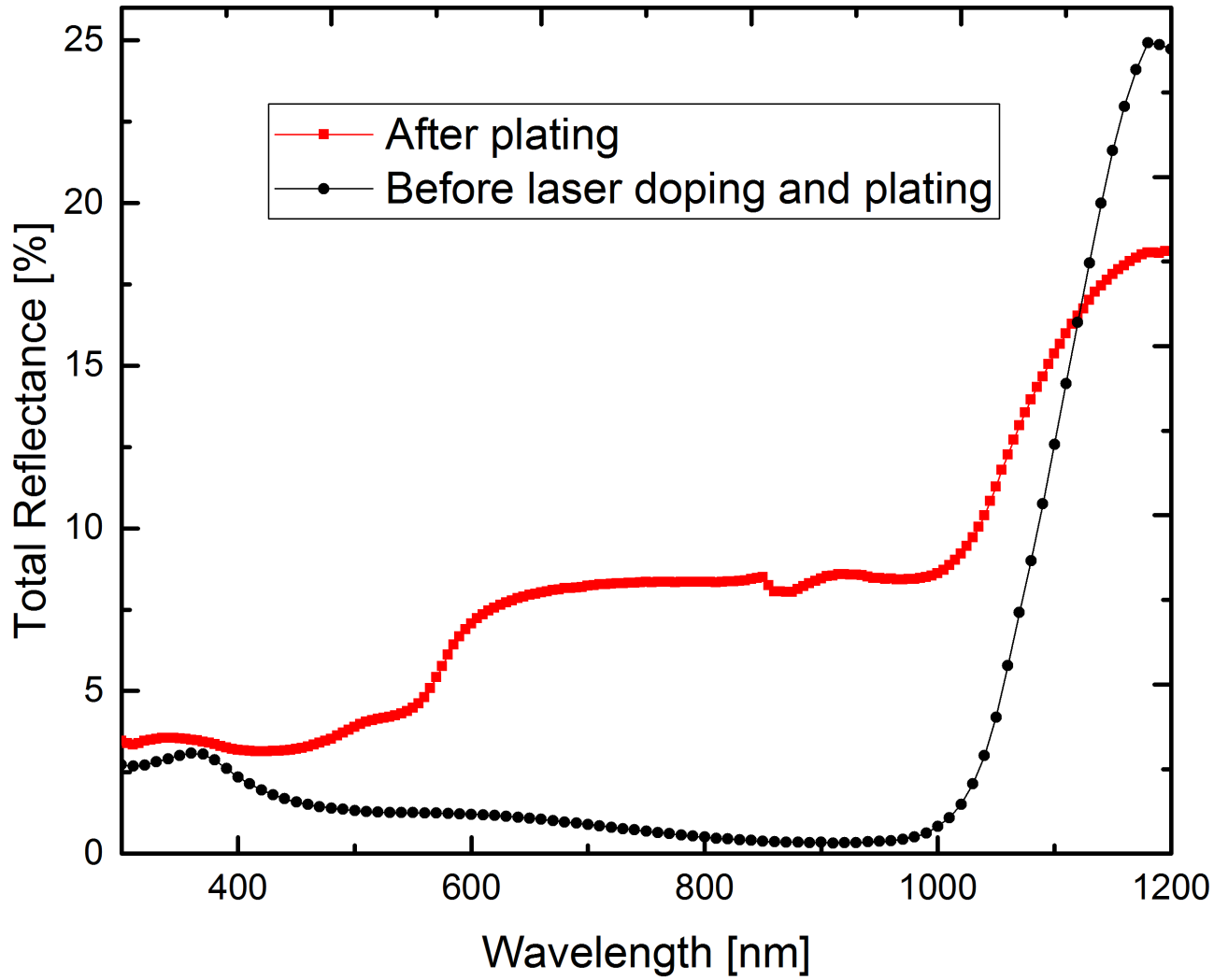


Figure 11: Total reflectance of the RIE-textured Si surface with AR-coating before and after laser doping and Ni/Cu-plating, respectively, as function of wavelength. The beam spot size of the light source was  $\sim 2$  cm in diameter and covered the majority of the cell area including the busbar and metal fingers.

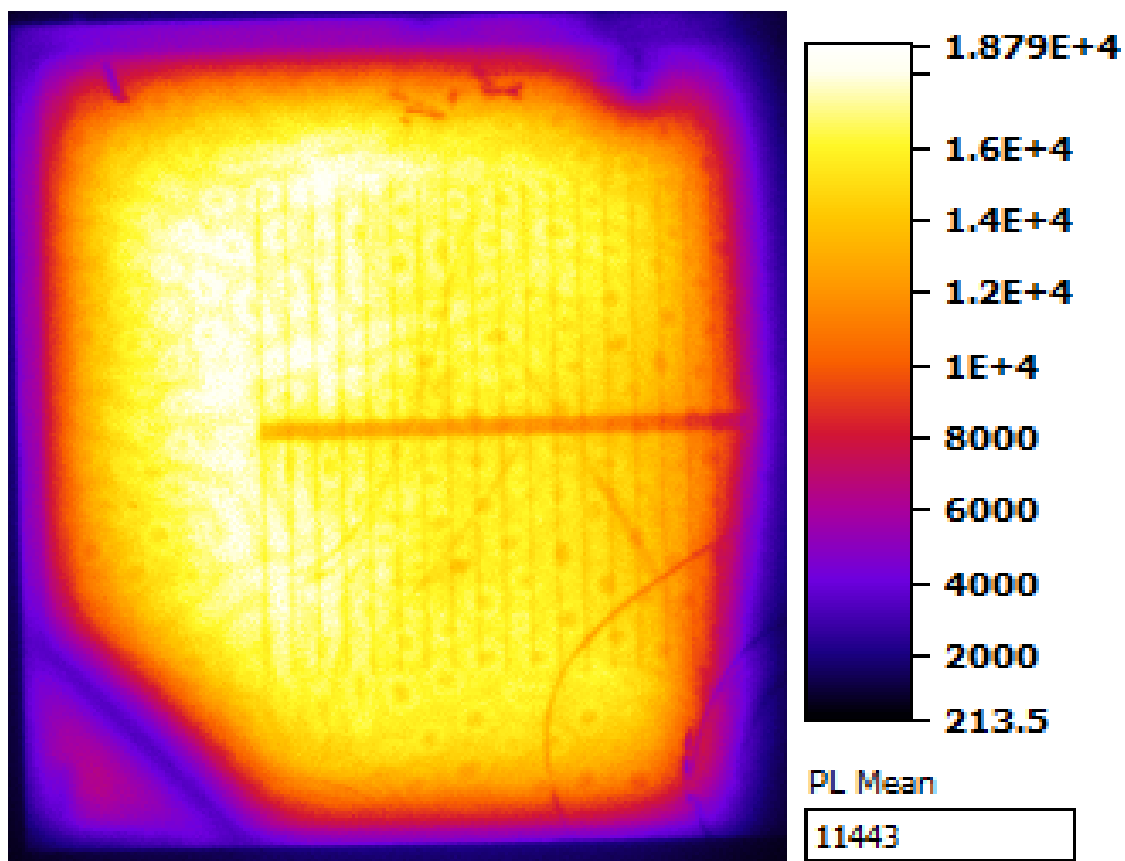


Figure 12: Open-circuit Photoluminescence (PL) image of the cell after Ni plating and sintering, but before Cu plating and edge isolation. The feature in the bottom left corner of the image is due to the shape of the screen-printed Al on the rear.

Author	Texturing	Eff.	$J_{SC}$	$V_{OC}$	FF	Cell Type
		[%]	[mA/cm <sup>2</sup> ]	[V]	[%]	Passivation, Cell Area
This work	RIE	18.1	36.3	0.624	80.1	CZ LDSE SiN <sub>x</sub> , 6.25 cm <sup>2</sup>
Repo <i>et al.</i> [17]	RIE	18.7	39.2	0.632	75.8	FZ PERL ALD Al <sub>2</sub> O <sub>3</sub> , 4 cm <sup>2</sup>
Yoo <i>et al.</i> [20]	RIE	16.7	36.8	0.617	76.0	CZ Screen-printed SiN <sub>x</sub> , 156.25 cm <sup>2</sup>
Oh <i>et al.</i> [19]	MACE*	18.2	36.5	0.628	79.6	FZ, evaporated contacts Thermal SiO <sub>2</sub> , 0.8081 cm <sup>2</sup>
Wang <i>et al.</i> [21]	MACE*	18.2	41.3	0.598	75.1	CZ, evaporated contacts ALD Al <sub>2</sub> O <sub>3</sub> , 0.92 cm <sup>2</sup>
Savin <i>et al.</i> [18]	RIE	22.1	42.2	0.665	78.7	FZ, IBC ALD Al <sub>2</sub> O <sub>3</sub> , 78.5 cm <sup>2</sup> (4")

Table 2: Selected black silicon solar cell results reported in literature. The table shows power conversion efficiency,  $J_{SC}$ ,  $V_{OC}$ , fill factor and type of solar cell and Si substrate. For further details about the cell type we refer to the references. \*Metal-Assisted Chemical Etching (MACE).